Proceedings of SIMS 50
Fredericia, Denmark
October 7–8, 2009

MODELLING A COMBINED HEAT AND POWER PLANT BASED ON GASIFICATION, MICRO GAS TURBINE AND SOLID OXIDE FUEL CELLS

Christian Bang-Møller* and Masoud Rokni
Technical University of Denmark
Department of Mechanical Engineering
2800 Kgs. Lyngby
Denmark

ABSTRACT

A system level modelling study on two combined heat and power (CHP) systems both based on biomass gasification. One system converts the product gas in a micro gas turbine (MGT) and the other in a combined solid oxide fuel cell (SOFC) and MGT arrangement. An electrochemical model of the SOFC has been developed and calibrated against published data from Topsoe Fuel Cells A/S (TOFC) and Risø National Laboratory, and the modelled gasifier is based on an up scaled version of the demonstrated low tar gasifier, Viking, situated at the Technical University of Denmark. The SOFC converts the syngas more efficient than the MGT reflected in the electrical efficiency of the gasifier and MGT system in opposition to the gasifier and SOFC-MGT configuration - η_{el}=28.1% versus η_{el}=50.3%.

Keywords: System modelling, biomass gasification, micro gas turbine, SOFC

NOMENCLATURE

a_{ohm}, b_{ohm}	coefficients for Eq. (24)
ASR	area specific resistance
E	reversible open circuit voltage
F	Faradays constant
g_f	Gibbs free energy of formation
i	current density
LHV	lower heating value
$\dot{n}$	molar flow
n_e	transferred electrons per molecule of fuel
p	pressure/partial pressure
P	power production
R	universal gas constant
T	temperature
UF	fuel utilization factor for SOFC
V	potential/overpotential
y	molar fraction
δ	SOFC layer thickness
η	efficiency

Subscripts:

a	anode
c	cathode
con	consumption
e	electrolyte
i	interconnect

INTRODUCTION

Development of sustainable and efficient production plants of combined heat and power (CHP) tends to gain more attention as climate changes, security of supply and depletion of fossil fuels have become well known issues. The share of biomass in CHP production are expected to increase in the future and decentralized CHP plants are also of interest to avoid costs of biomass transportation. Efficient power producing technologies for small scale productions are typically gas engines, micro gas turbines (MGT) and fuel cells – all requiring gaseous fuel. Gasification can deliver biomass based gaseous fuel so the combination of biomass gasification and efficient syngas conversion are potentially a sustainable and efficient CHP plant.

Solid oxide fuel cells (SOFCs) can electrochemically convert H_2 and CO as well as internally reform CH_4 into more H_2 and CO due to their high operating temperature. This makes SOFCs very fuel flexible and ideal for converting syngas compared to other fuel cell types.

The performance and system design of integrated biomass gasifier and SOFC systems in the 100-

* Corresponding author: Email: chrbm@win.dtu.dk Phone: +45 45254123

1000kW$_e$ class have been investigated by several. An innovative design including heat pipes between a SOFC stack and an allothermal gasifier is described in [1]. Fryda et al. [2] studies the performance of a CHP system of less than 1MW$_e$ and consisting of an autothermal gasifier combined with a MGT and/or SOFC.

This study focus on the performance of a system combining an up scaled version (~500kW$_{th}$) of the two-stage gasifier named Viking and a MGT or a SOFC-MGT system. Viking is a 75kW$_{th}$ autothermal (air blown) fixed bed biomass gasifier demonstrated at the Technical University of Denmark and it is described in detail in [3]. The Viking gasifier produces almost no tars, which is favourable for downstream SOFC operation. Hofmann et al. [4] has operated a SOFC on cleaned syngas from the Viking gasifier for 150 hours without degradation.

The present study is based on zero dimensional and steady-state modelling in the simulation tool DNA [5]. DNA has incorporated thermodynamic property data, is component based and is developed at The Technical University of Denmark.

SYSTEM DESCRIPTION

Two different combined heat and power systems are investigated in this study, both based on syngas production from an up scaled Viking gasifier. A flow sheet of the two systems is depicted in Figure 1. The modelled gasifier system is slightly simplified, but aims at the same resulting gas composition and cold gas efficiency as for the Viking gasifier. In the gasifier model the dryer is heated by hot syngas. The steam production from the dryer is added to the preheated air and dry wood and mixed air and steam are fed to the gasifier. The raw product gas are cooled to 90°C in three steps; air preheating, wood drying and syngas cooling producing hot water for district heating. The cooled syngas are then cleaned from impurities as particles and sulphur compounds before some of the water in the gas are condensed through cooling to 50°C. The cleaned and partly dried syngas are then converted into electricity and heat in a bottoming cycle consisting of a MGT or both a SOFC and a MGT. These two system configurations will from now on be referred as the Gasifier-MGT and the Gasifier-SOFC-MGT configuration, respectively. In the Gasifier-SOFC-MGT configuration all the components in the flow sheet are in use. With respect to Figure 1 the SOFC and preheaters are bypassed in the Gasifier-MGT arrangement. In addition the syngas compressor works as a roots blower for the gasifier system and not illustrated is a generator.

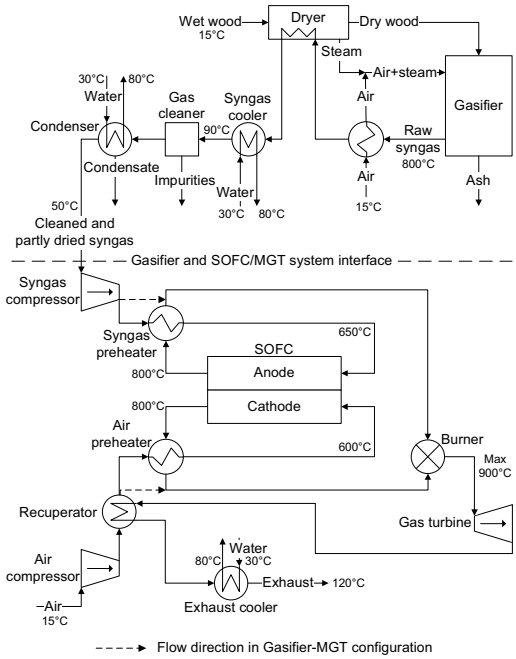

Figure 1: Flow sheet of the hybrid systems

Operating pressure	$p_{gasifier}$	0.998 bar
Operating temperature	$T_{gasifier}$	800°C
Pressure loss	$\Delta p_{gasifier}$	5 mbar
Non-equilibrium methane	*METH*	0.01

Table 1: Inputs to the gasifier submodel

GASIFIER MODEL

The gasifier component calculates the produced syngas composition as well as the produced ashes based on the inlet media composition and the operating conditions. The input parameters defining the operating conditions for the gasifier submodel are given in Table 1. The gasifier pressure loss is defined as the difference between the inlet air and steam mixture and the outlet syngas.

In the gasifier the incoming flows are converted into a syngas and ashes. The ashes come from a defined content in the biomass. The syngas can consist of the following species: H_2, O_2, N_2, CO,

NO, CO_2, H_2O, NH_3, H_2S, SO_2, CH_4, NO_2, HCN, COS and Ar. It is assumed that equilibrium is reached at the operating temperature and pressure, where the total Gibbs energy has its minimum value. With this assumption the syngas outlet composition can be found by the Gibbs minimization method [6]. A possibility for bypassing an amount of methane from the equilibrium calculations is added in order to reach syngas compositions, which contain more methane than the corresponding one at equilibrium. Thus the syngas composition can be adjusted to match real syngas compositions, e.g. from the Viking gasifier. The input parameter *METH* is used for this bypassing and is defined as the fraction of the methane that is not included in the equilibrium calculations and instead flows through the gasifier and appears in the outlet syngas.

Gasifier model validation

The model validation for the gasifier is done for all of the gasification plant from the biomass input to the cleaned and dried syngas. Thus the data from the Viking gasifier plant can be used for validation.

Wood chips from beech with small amounts of oak are used in the modelling as for the Viking gasifier reported in Ahrenfeldt et al. [3].

As seen in Table 2 the produced syngas composition and the lower heating value (LHV) from the gasifier model is close to the Viking data. The overall performance of the modelled gasifier is also similar to the Viking gasifier expressed in the cold gas efficiencies.

	Viking [3]	Gasifier model
H_2 (vol-%)	30.5	29.9
CO (vol-%)	19.6	20.8
CO_2 (vol-%)	15.4	13.5
CH_4 (vol-%)	1.16	1.19
N_2 (vol-%)	33.3	34.2
LHV (MJ/kg)	6.2	6.3
Cold gas eff.	93%	94%

Table 2: Dry syngas composition, lower heating value as well as cold gas efficiency for the Viking gasifier and the modelled gasifier, respectively

Fuel utilization factor	UF	0.85
Operating temperature	T_{SOFC}	800°C
Anode pressure loss	Δp_a	5 mbar
Cathode pressure loss	Δp_c	10 mbar
Current density	i	300 mA cm^{-2}

Table 3: Inputs to the SOFC submodel

SOLID OXIDE FUEL CELL MODEL

The SOFC stack component calculates the air and fuel outlet compositions as well as the power production. The calculations are based on the inlet air and fuel compositions and flow rates as well as the other operating conditions of the SOFC. The SOFC submodel includes an electrochemical model for predicting the performance of the SOFC. The operating conditions are partly described by input parameters given to the SOFC submodel and these are presented in Table 3.

In the submodel only H_2 is electrochemically converted in the SOFC anode, but the model takes into account that CO produces an extra H_2 through the water-gas-shift (WGS) reaction, while four additional H_2 molecules are produced from CH_4 through internal steam reforming and WGS of produced CO (full conversion is assumed). The total mole flow of H_2 on the anode after internal steam reforming and WGS is expressed in Eq. (1).

$$\dot{n}_{H_2,tot} = \dot{n}_{H_2,in} + \dot{n}_{CO,in} + 4\dot{n}_{CH_4,in} \quad (1)$$

$$H_2 + O^{2-} \rightarrow H_2O + 2e^- \quad (2)$$

$$\tfrac{1}{2}O_2 + 2e^- \rightarrow O^{2-} \quad (3)$$

$$H_2 + \tfrac{1}{2}O_2 \rightarrow H_2O \quad (4)$$

The amount of hydrogen that is converted depends on the fuel utilization factor (*UF*) and this amount is electrochemically converted in the anode. The electrode reactions and the overall fuel cell reaction are as shown in Eq. (2) to (4).

From the overall fuel cell reaction it is seen that the amount of consumed oxygen is half the amount of consumed hydrogen. The cathode outlet composition can then be found by the following equations if the only species taking into account are O_2, N_2, CO_2, H_2O and Ar.

$$\dot{n}_{O_2,con} = \frac{UF\dot{n}_{H_2,in}}{2} \quad (5)$$

$$\dot{n}_{c,out} = \dot{n}_{c,in} - \dot{n}_{O_2,con} \quad (6)$$

$$y_{O_2,\text{out}} = \frac{\dot{n}_{\text{c,in}} y_{O_2,\text{in}} - \dot{n}_{O_2,\text{con}}}{\dot{n}_{\text{c,out}}} \quad (7)$$

$$y_{j,\text{out}} = \frac{\dot{n}_{\text{c,in}} y_{j,\text{in}}}{\dot{n}_{\text{c,out}}}, \; j = \{N_2, CO_2, H_2O\} \quad (8)$$

$$y_{\text{Ar,out}} = 1 - y_{O_2,\text{out}} - y_{N_2,\text{out}} - y_{CO_2,\text{out}} - y_{H_2O,\text{out}} \quad (9)$$

The fuel composition leaving the anode is calculated by the Gibbs minimization method [6] as described for the gasifier submodel. Equilibrium at the anode outlet temperature and pressure is assumed for the following species: H_2, CO, CO_2, H_2O, CH_4 and N_2. The equilibrium assumption is fair since the methane content in this study is low enough for such kind of assumption to be made. The heat consumed by the endothermic internal reforming reactions is taken into account by the Gibbs minimization method. More internal reforming means more cooling of the SOFC.

The power production from the SOFC depends on the amount of chemical energy fed to the anode, the reversible efficiency (η_{rev}), the voltage efficiency (η_{v}) and the fuel utilization factor (UF). It is defined in mathematical form in Eq. (10).

$$P_{\text{SOFC}} = \begin{bmatrix} LHV_{H_2}\dot{n}_{H_2,\text{in}} \\ + LHV_{CO}\dot{n}_{CO,\text{in}} \\ + LHV_{CH_4}\dot{n}_{CH_4,\text{in}} \end{bmatrix} \eta_{\text{rev}}\eta_{\text{v}} UF \quad (10)$$

The reversible efficiency is the maximum possible efficiency defined as the relationship between the maximum electrical energy available (change in Gibbs free energy) and the fuels LHV. This is shown in Eq. (11) and the definition of the change in Gibbs free energy is shown in Eq. (12). The voltage efficiency express the electrochemical performance of the SOFC and the calculation of the voltage efficiency is described in the following subsection.

$$\eta_{\text{rev}} = \frac{(\Delta\bar{g}_{\text{f}})_{\text{fuel}}}{LHV_{\text{fuel}}} \quad (11)$$

$$\begin{aligned}(\Delta\bar{g}_{\text{f}})_{\text{fuel}} = & \left[(\bar{g}_{\text{f}})_{H_2O} - (\bar{g}_{\text{f}})_{H_2} - \tfrac{1}{2}(\bar{g}_{\text{f}})_{O_2}\right] y_{H_2,\text{in}} \\ & + \left[(\bar{g}_{\text{f}})_{CO_2} - (\bar{g}_{\text{f}})_{CO} - \tfrac{1}{2}(\bar{g}_{\text{f}})_{O_2}\right] y_{CO,\text{in}} \\ & + \left[(\bar{g}_{\text{f}})_{CO_2} + 2(\bar{g}_{\text{f}})_{H_2O} - (\bar{g}_{\text{f}})_{CH_4} - 2(\bar{g}_{\text{f}})_{O_2}\right] y_{CH_4,\text{in}}\end{aligned} \quad (12)$$

Electrochemical model

The electrochemical model is used to calculate the cell potential and the voltage efficiency of the SOFC. Both depend on the operating conditions such as temperature, pressure, gas compositions, fuel utilization and load (current density). The cell potential and voltage efficiency is defined in Eq. (13) and (14), respectively.

$$V_{\text{cell}} = E - V_{\text{act}} - V_{\text{ohm}} \quad (13)$$

$$\eta_{\text{v}} = \frac{V_{\text{cell}}}{E} \quad (14)$$

In the following the reversible open circuit voltage (E), the activation overpotential (V_{act}) and the ohmic overpotential (V_{ohm}) are calculated. Traditionally a concentration overpotential term is included in Eq. (13). The concentration overpotential is a result of the limitations of transporting the reactants to the active cell area. In Larminie et. al. [7] it is described as a voltage drop caused by the pressure change associated with the consumption of reactants. As a result of the current being drawn from the cell the average partial pressure of reactants is lower than at the inlet. Thus, in this study the concentration overvoltage is taken into account by using average partial pressures when calculating E and V_{act}.

E can be calculated from the Nernst equation:

$$E = \frac{-\Delta\bar{g}_{\text{f}}^{\,0}}{n_{\text{e}}F} + \frac{RT}{n_{\text{e}}F}\ln\left(\frac{\bar{p}_{H_2,\text{tot}}\sqrt{\bar{p}_{O_2}}}{\bar{p}_{H_2O}}\right) \quad (15)$$

Since it is assumed that all CO and CH_4 are converted to H_2 before the electrochemical reactions takes place, the change in standard Gibbs free energy ($\Delta\bar{g}_{\text{f}}^{\,0}$) and the number of electrons transferred for each molecule of fuel (n_{e}) is determined for the reaction of H_2 only. Thus, n_{e} = 2 and $\Delta\bar{g}_{\text{f}}^{\,0} = (\bar{g}_{\text{f}}^{\,0})_{H_2O} - (\bar{g}_{\text{f}}^{\,0})_{H_2} - \tfrac{1}{2}(\bar{g}_{\text{f}}^{\,0})_{O_2}$. The partial pressure of species j is an average across the respective electrode and is here defined as an arithmetic mean between inlet and outlet as shown in Eq. (16) and (17). The average partial pressure of available hydrogen after internal steam reforming and WGS of CH_4 and CO can be determined from

the overall steam reforming and WGS reaction including all species. It is defined in Eq. (18):

$$\overline{p}_j = \left(\frac{y_{j,\mathrm{out}} - y_{j,\mathrm{in}}}{2} \right) p_\mathrm{a}\,, \tag{16}$$

$$j = \{\mathrm{H_2, CO, CH_4, CO_2, H_2O, N_2}\}$$

$$\overline{p}_{\mathrm{O_2}} = \left(\frac{y_{\mathrm{O_2,out}} - y_{\mathrm{O_2,in}}}{2} \right) p_\mathrm{c} \tag{17}$$

$$\overline{p}_{\mathrm{H_2,tot}} = \left(\frac{\overline{p}_{\mathrm{H_2}} + \overline{p}_{\mathrm{CO}} + 4\overline{p}_{\mathrm{CH_4}}}{\overline{p}_{\mathrm{H_2}} + \overline{p}_{\mathrm{CO}} + 3\overline{p}_{\mathrm{CH_4}} + \overline{p}_{\mathrm{CO_2}} + \overline{p}_{\mathrm{H_2O}} + \overline{p}_{\mathrm{N_2}}} \right) p_\mathrm{a} \tag{18}$$

The activation overpotential is due to an energy barrier (activation energy) that the reactants must overcome in order to drive the electrochemical reactions. The activation overpotential is non-linear and is dominant at low current density (i). The activation overpotential is defined as (cf. [8]):

$$\begin{aligned} V_\mathrm{act} &= V_\mathrm{act,a} + V_\mathrm{act,c} \\ &= \frac{2RT}{n_\mathrm{e}F} \left[\sinh^{-1}\left(\frac{i + i_\mathrm{n}}{2i_{0,\mathrm{a}}} \right) + \sinh^{-1}\left(\frac{i + i_\mathrm{n}}{2i_{0,\mathrm{c}}} \right) \right] \end{aligned} \tag{19}$$

The internal current density (i_n) is added to the actual fuel cell current density in order to account for the mixed potential caused by fuel crossover. The importance of the internal current density in the case of SOFCs is much less than for low temperature fuel cells and the value of i_n is usually very small [7]. The exchange current density (i_0) is a measure of the level of activity on the electrode at i=0 mA cm^{-2} and is defined as (cf. [9]):

$$i_{0,\mathrm{a}} = 2.13 \times 10^7 \left(\frac{\overline{p}_{\mathrm{H_2,tot}} \overline{p}_{\mathrm{H_2O}}}{p_\mathrm{a}^{\,2}} \right) \exp\left(\frac{-110000}{RT} \right) \tag{20}$$

$$i_{0,\mathrm{c}} = 1.49 \times 10^7 \left(\frac{\overline{p}_{\mathrm{O_2}}}{p_\mathrm{c}} \right)^{0.25} \exp\left(\frac{-110000}{RT} \right) \tag{21}$$

The ohmic overpotential is caused by the electrical resistance for the ions passing through the electrolyte as well as for the electrons passing through the electrodes and interconnects. The

R	8.314 J K^{-1} mol^{-1}	
F	96485 C mol^{-1}	
n_e	2	
i_n	2 mA cm^{-2}	[9]
δ_a	750×10^{-4} cm	[10]
δ_c	50×10^{-4} cm	[10]
δ_e	40×10^{-4} cm	[10]
δ_i	100×10^{-4} cm	[11]
$a_\mathrm{ohm,a}$	0.00298×10^{-3} kΩcm	[12]
$b_\mathrm{ohm,a}$	-1392 K	[12]
$a_\mathrm{ohm,c}$	0.00811×10^{-3} kΩcm	[12]
$b_\mathrm{ohm,c}$	600 K	[12]
$a_\mathrm{ohm,e}$	0.00294×10^{-3} kΩcm	[12]
$b_\mathrm{ohm,e}$	10350 K	[12]
$a_\mathrm{ohm,i}$	0.1256×10^{-3} kΩcm	[12]
$b_\mathrm{ohm,i}$	4690 K	[12]

Table 4: Inputs for the electrochemical model

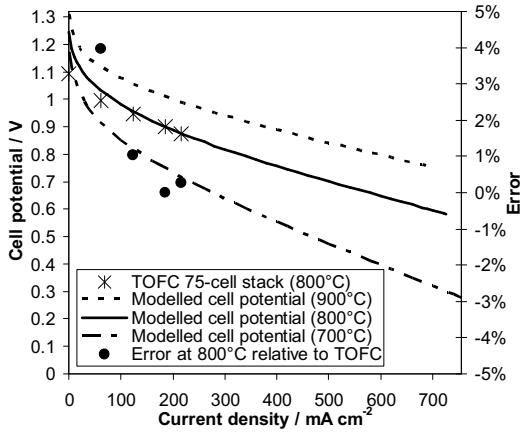

Figure 2: Single cell polarization curves based on a 75-cell stack and the SOFC model, respectively.

ohmic overpotential is defined below (cf. [9] and [12]).

$$V_\mathrm{ohm} = i\,ASR \tag{22}$$

$$ASR = ASR_\mathrm{a} + ASR_\mathrm{c} + ASR_\mathrm{e} + ASR_\mathrm{i} \tag{23}$$

$$ASR_j = \delta_j a_{\mathrm{ohm},j} \exp\left(\frac{b_{\mathrm{ohm},j}}{T} \right),\ j = \{\mathrm{a,c,e,i}\} \tag{24}$$

The thicknesses of the different layers (δ) and the constants a_ohm and b_ohm used are listed in Table 4.

SOFC model calibration

The described electrochemical model has been calibrated against experimental data. Since the model aims at the performance of 2nd generation SOFCs from Topsoe Fuel Cell A/S (TOFC) and Risø National Laboratory, published data from this SOFC type has been used. The *ASR* has been calibrated against a value of 0.15 Ω cm^2 at 850°C as published by [13] and the resulting cell potential has been calibrated against a polarization curve (800°C and fuelled with H_2 and N_2) published by [14]. An active cell area of 81 cm^2 has been assumed. Both modelled and experimental data as well as the error relative to the experimental data are presented in Figure 2.

The model shows excellent agreement with the experimental data above a current density of 100 mA cm^{-2}. The current density of 300 mA cm^{-2} is chosen to represent the SOFC load in the following results.

PERIPHERAL EQUIPMENT

Modelling of peripheral components like compressors, turbines and heat exchangers are standard and therefore not described in detail.

The throughput of wet biomass is 154.8 kg h^{-1} (corresponds to 499.2 kW_{th} (LHV)). Thus it is assumed that the Viking gasifier can be scaled up from a nominal ~75 kW_{th} [3]. The biomass dryer reduces the water content in the biomass from 32.2 wt-% to 5 wt-% by heating it to 150°C and the air for the gasifier is preheated to 780°C by the hot product gas.

The inlet temperature to the SOFC anode and cathode are maintained at 150°C and 200°C below the outlet temperature, respectively.

The pressure loss in every component in the SOFC air supply stream and burner exhaust stream is assumed to be 10 mbar, while the pressure loss in each of the rest of the components is assumed to be 5 mbar, except the burner that has a pressure loss of 0.6‰ (equals 1.5 mbar when 2.5 bar at inlet).

The gas cleaner is a baghouse filter removing particulates and it is assumed that the cleaned syngas can be used directly in a SOFC. The condenser removes some of the water content in the syngas resulting in a content of water in the cleaned and dried syngas of 12.7 vol-%. The resulting steam to carbon ratio (S/C) is 0.41, which is somewhat low, but is justified by the very low tar content in the Viking syngas.

The isentropic and mechanical efficiency of the compressors are 75% and 98%, respectively, and the isentropic efficiency of the MGT expander is 84%. The turbine inlet temperature (TIT) is limited to 900°C in the Gasifier-MGT case, while varied in the Gasifier-SOFC-MGT arrangement. The performance of the compressors and the MGT expander are taken from Fryda et al. [2] and corresponds to common performance data for a MGT of this scale. The recuperator effectiveness is assumed to be 85% and the generator efficiency is assumed to be 99%. In the Gasifier-MGT configuration the burner operating pressure is 3.75 bar and in the Gasifier-SOFC-MGT case the SOFC operating pressure is 2.5 bar (these pressures are varied in the results section).

No heat losses are taken into account. Introducing heat losses from the gas cleaner will only affect the heat production from the condenser since the temperature after the condenser is fixed to 50°C.

The outlet pressure from the MGT depends on the total pressure loss downstream the MGT, since it is the exhaust pressure which is fixed to 1.013 bar. Because of the recuperator and exhaust cooler the outlet pressure from the MGT is 1.033 bar. The district heating (DH) water is assumed to be 30°C at inlet and 80°C at outlet.

RESULTS AND DISCUSSION

In the following results the inputs presented in the previous sections are used unless something else is stated. The system configurations are previously described in detail.

The performance of the different system configurations vary greatly with the operating conditions and namely the pressure ratio of the MGT (in the Gasifier-MGT case) and the operating pressure of the SOFC (in the Gasifier-SOFC-MGT case) are of great importance to the resulting system performance. The two system configurations have different optimum with regard to their operating pressure and these can be seen in Figure 3. When operating at a constant TIT of 900°C the Gasifier-MGT configuration shows an optimum at 3.75 bar performing an electric efficiency of 28.1%. It is the recuperator that ensures an optimum at a rela-

tively low operating pressure. By combining the SOFC and MGT in the Gasifier-SOFC-MGT configuration the electrical efficiency reaches 50.3% at an optimum operating pressure of 2.5 bar. This is a substantial increase in efficiency caused by the efficient SOFC. With a fuel utilization of 85% a part of the fuel passes through the anode, but this amount is used in the MGT. In this case the TIT is varying with the SOFC operating pressure and has a value of 697°C at 2.5 bar.

The Gasifier-MGT system performance also depend on the allowed TIT as depicted in Figure 4. Decreasing the TIT by 100°C to 800°C lowers the electrical efficiency to 25.4% - a drop of 2.7 percentage points. In the Gasifier-SOFC-MGT configuration a drop in SOFC operating temperature by 100°C to 700°C decreases the electrical efficiency to 44.4% - a drop of 5.9 percentage points. This indicates that the SOFC operating temperature has more influence on the SOFC performance than the TIT has on the MGT performance. The research and development working on lowering the SOFC operating temperature in order to use cheaper materials will influence the system performance presented here and potentially other bottoming cycles could be beneficial, e.g. a Rankine cycle.

The sensitivity of the model results to the chosen SOFC current density is shown in Figure 5. At the reference current density value of 300 mA cm^{-2} the SOFC voltage efficiency (defined in Eq. (14)) is 40.8%. Raising the SOFC load to 500 mA cm^{-2} lowers the voltage efficiency to 35.7% meaning a reduction in the total electrical efficiency to 46.7% - a drop of 3.6 percentage points. This is a relative change in electrical efficiency of 7% for a 66.7% increase in current density.

Key data for the two system configurations studied are presented in Table 5 and the respective optimal operating pressure is used in each configuration as well as the reference input values presented in the previous sections. The Gasifier-SOFC-MGT configuration clearly has the best electrical efficiency, while the CHP efficiencies do not differ significantly. In the Gasifier-SOFC-MGT case, the power production is mainly from the SOFC producing 76.4% of the power. The exact values of the efficiencies will be slightly lower when incorporating heat losses, a more accurate efficiency of the gasifier system and possible more extensive gas cleaning, but the comparison of the systems performance is still valid.

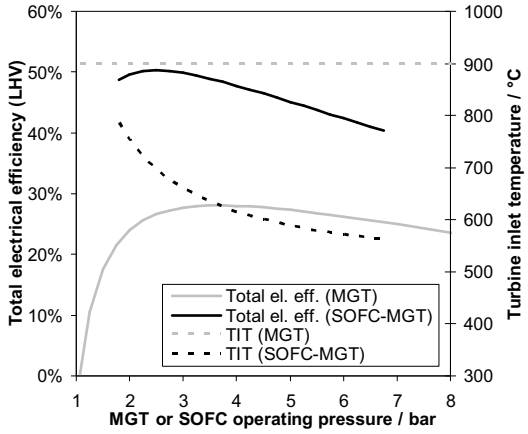

Figure 3: Electric efficiency and TIT at different MGT or SOFC operating pressures

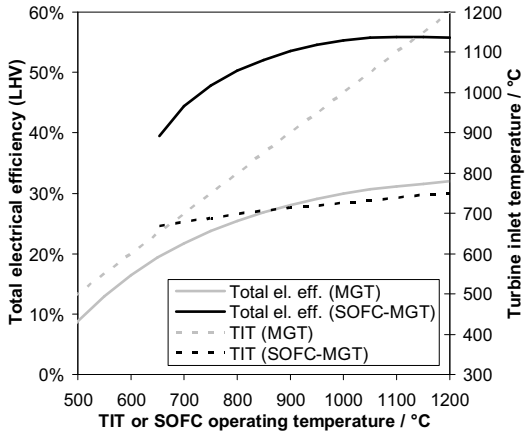

Figure 4: Electric efficiency and TIT at different TIT or SOFC operating temperatures

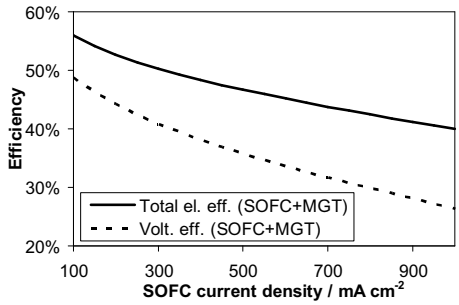

Figure 5: Electrical efficiency and SOFC voltage efficiency as a function of SOFC current density

		Gasifier -MGT	Gasifier -SOFC-MGT
Biomass input	/ kg h^{-1}	154.8	154.8
	/ $kW_{th,LHV}$	499.2	499.2
p_{MGT} or p_{SOFC} / bar		3.75	2.5
$P_{MGT,net}$ / kW_{el}		140.1	59.2
$P_{SOFC,net}$ / kW_{el}		-	191.8
$P_{total,net}$ / kW_{el}		140.1	251.0
DH production / kJ s^{-1}		239.7	146.7
η_{el} / % (LHV)		28.1	50.3
η_{CHP} / % (LHV)		76.1	79.7

Table 5: Key data for the studied systems

CONCLUSION

A study on the system performance of an up scaled Viking gasifier (~500 kW_{th}) with either a downstream MGT or SOFC-MGT has been conducted by zero dimensional process modelling. A SOFC submodel has been developed including an electrochemical model predicting the SOFC performance at different operating conditions. This submodel has been calibrated against published TOFC stack performance data. The reference conditions for the SOFC has been an operating temperature of 800°C, a fuel utilization of 85% and a current density of 300 mA cm^{-2}. The optimal operating MGT and SOFC-MGT pressure has been found for the two system configurations to 3.75 and 2.5 bar, respectively. The SOFC converted the syngas more efficient than the MGT reflected in the efficiency of the gasifier and MGT system configuration in opposition to the gasifier and SOFC-MGT configuration - η_{el}=28.1% versus η_{el}=50.3%. These efficiencies were very sensitive to the SOFC operating temperature (or TIT in the Gasifier-MGT arrangement), while only a moderate sensitivity to the SOFC current density was observed.

REFERENCES

[1] Karellas S, Karl J, Kakaras E. *An innovative biomass gasification process and its coupling with microturbine and fuel cell systems*. Energy 2008;33:284–291.

[2] Fryda L, Panopoulos KD, Kakaras E. *Integrated CHP with autothermal biomass gasification and SOFC–MGT*. Energy Conversion and Management 2008;49:281–290.

[3] Ahrenfeldt J, Henriksen U, Jensen TK, Gøbel B, Wiese L, Kather L, Egsgaard H. *Validation of a Continuous Combined Heat and Power (CHP) Operation of a Two-Stage Biomass Gasifier*. Energy & Fuels 2006;20:2672-2680.

[4] Hofmann Ph, Schweiger A, Fryda L, Panopoulos KD, Hohenwarter U, Bentzen JD, Ouweltjes JP, Ahrenfeldt J, Henriksen U, Kakaras E. *High temperature electrolyte supported Ni-GDC/YSZ/LSM SOFC operation on two-stage Viking gasifier product gas*. J. Power Sources 2007;173:357–366.

[5] Elmegaard B, Houbak N. *DNA – A General Energy System Simulation Tool*, In: Proceedings of the 46th Conf. on Simulation and Modeling, Trondheim, 2005. (cf. http://www.scansims.org/sims2005)

[6] Smith JM, Van Ness HC, Abbott MM. *Introduction to Chemical Engineering Thermodynamics*. 7th ed. Boston: McGraw-Hill, 2005.

[7] Larminie J, Dicks A. *Fuel Cell Systems Explained*. 2nd ed. West Sussex: John Wiley & Sons Ltd., 2003.

[8] Aloui T, Halouani K. *Analytical modeling of polarizations in a solid oxide fuel cell using biomass syngas product as fuel*. Appl. Therm. Eng. 2007;27:731-737.

[9] Calise F, Dentice d'Accadia M, Palombo A, Vanoli L. *Simulation and exergy analysis of a hybrid Solid Oxide Fuel Cell (SOFC)–Gas Turbine System*. Energy 2006;31:3278-3299.

[10] Chan SH, Khor KA, Xia ZT. *A complete polarization model of a solid oxide fuel cell and its sensitivity to the change of cell component thickness*. J. Power Sources 2001;93:130-140.

[11] Chan SH, Low CF, Ding OL. *Energy and exergy analysis of simple solid-oxide fuel-cell power systems*. J. Power Sources 2002;103:188-200.

[12] Bessette NF II, Wepfer WJ, Winnick J. *A Mathematical Model of a Solid Oxide Fuel Cell*. J. Electrochem. Soc. 1995;142:3792-3800.

[13] Christiansen N, Hansen JB, Holm-Larsen H, Linderoth S, Larsen PH, Hendriksen PV, Mogensen M. *Solid oxide fuel cell development at Topsoe Fuel Cell and Risø*. Fuel Cells Bulletin 2006;2006(8):12-15.

[14] Linderoth S, Larsen PH, Mogensen M, Hendriksen PV, Christiansen N, Holm-Larsen H. *Solid Oxide Fuel Cell (SOFC) Development in Denmark*. Materials Science Forum 2007;539-543:1309-1314.